Advanced Journal of Chemistry, Section A, 2024, 7(5), 550-564

Advanced Journal of Chemistry, Section A

Journal homepage: www.ajchem-a.com

Original Research Article

Fabrication of Electrochemically Deposited Zinc Rich Ni-Co-Zn Alloy Coatings Reinforced with Pyridine and Investigation of Their Anticorrosion Performance in Acidic Mediums

Shraddha Bais*

Department of Chemistry, Institute of Science and Research, IPS Academy, Indore (M.P.) 452012, India

ARTICLEINFO

Article history

Submitted: 06 March 2024
Revised: 24 April 2024
Accepted: 26 May 2024

Manuscript ID: AJCA-2404-1508
Checked for Plagiarism: Yes
Language Editor Checked: Yes
DOI: **10.48309/AJCA.2024.450766.1508**

KEYWORDS

Galvanostatic deposition
Corrosion inhibitor
Anticorrosive coating
Corrosion protection

ABSTRACT

The immense corrosion rate of NiCo alloy coatings is the main problem to use it as constructive material. A study was carried out to synthesize Zn rich Ni-Co-Zn alloy coatings prepared on mild steel substrate with and without addition of Pyridine in deposition medium to test the effect of pyridine addition on corrosion of deposited alloy coatings. Galvanostatic electrodeposition technique was used to deposit alloy coatings on to the mild steel substrate at a fix current density of 4 mA/cm^2. All 4 coatings prepared from 4 different deposition baths showed excellent surface coverage on Mild steel substrate. The alloy coatings were characterized by SEM, EDAX and XRD. The SEM analysis revealed the presence of cauliflower shaped agglomerated particles which are asymmetrically distributed throughout the surface. The XRD analysis confirmed the formation of alloy which is crystalline in nature and having η Zn-Ni as predominant phase along with the ηZn, ZnO and Co_3O_4 Crystalline phase in all the coatings. The strain of the coatings was calculated using Williamson-Hall Plot. The anticorrosive performance of Ni-Co-Zn alloy coatings prepared in absence and presence of pyridine from different deposition baths were compared by potentiodynamic polarization measurement using tafel plot. The pyridine acts as moderate corrosion inhibitor and enhanced the corrosion resistance of the coatings. The comparative analysis of coatings obtained from DB1 and DB3 showed the percentage inhibitor efficacy of 36.91% in 0.01 M HCl medium and 36.94% in 0.01 M H_2SO_4 medium. The inhibitor efficacy of coating obtained from DB4 when compared with the coating obtained from DB2, it is higher in HCl medium (66.48%) as compared to H_2SO_4 medium (40.42%).

* Corresponding author: Bais, Shraddha
✉ E-mail: shradha.bais@gmail.com

GRAPHICAL ABSTRACT

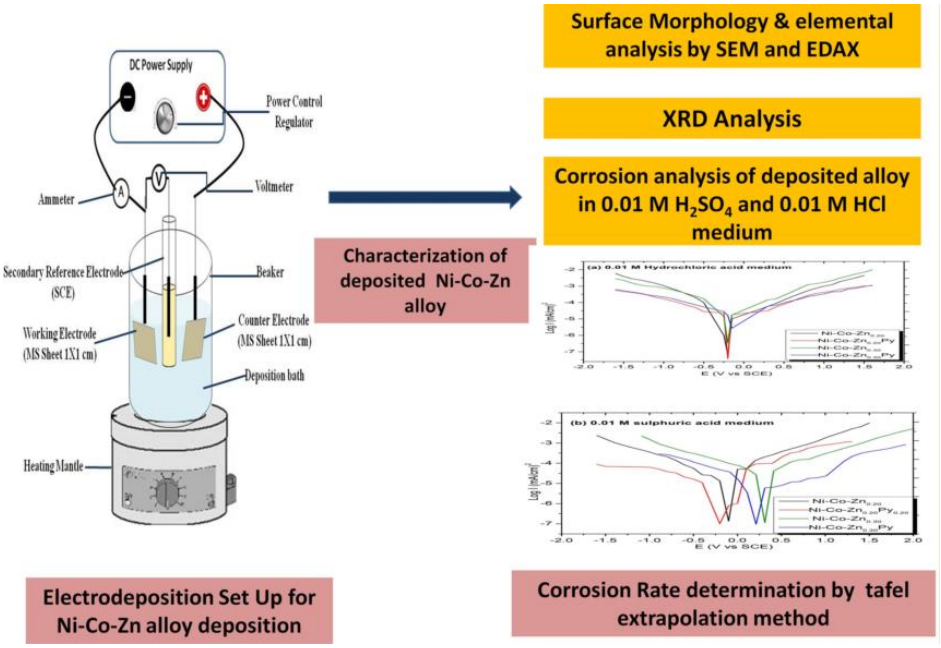

Introduction

Anticorrosion transition metal alloys [1-3] are gaining remarkable interest of scientific community due to its significant applications in aviation industry, automobile industries [4], chemical process industry, marine industry, etc. Many researchers deliberated the corrosion performance of Ni-Co alloys [5,6] and Zn-Ni alloys [7-9] and found them suitable for anticorrosive purpose. Alloys with much lower corrosion rate are predicted to be appropriate for practical application. To fabricate anticorrosive alloys a large number of techniques are implemented, including chemical bath deposition [10,11], pulsed laser deposition [12,13], powder metallurgy [14,15], hydrothermal synthesis [16], etc. All these techniques are time consuming and expensive due to special reagent requirements, manufacturing conditions, and specific instrument requirements whereas the electrochemical deposition [17-20] is considered as cost effective and prominent technique for the alloy synthesis by which we can construct alloys of desired composition with controlled microstructure. The concept of corrosion inhibitors [21-24] is attaining very much interest of contemporary scientific community for superior the corrosion defense of metals, alloys and their coatings. A corrosion inhibitor is a matter when introduce in a minute concentration to an environment lessen the corrosion rate of a metal or alloy exposed to that environment. It can be use either internal addition into the plating bath as additive [25-28] or by addition in exposing environment [29-31]. Organic compounds containing nitrogen, oxygen and sulphur reduces the corrosion rate [32]. Inhibitors act by selectively precipitating on cathodic or anodic or mixed areas to limit the diffusion of reducing species to the surface [33].

Mild steel is one of the most important engineered materials used in steel frame buildings, structural fabrication, machinery parts, pipelines, etc. However, the main problem with mild steel or low carbon steel is corrosion by surrounding environmental conditions so it is an important task to prevent mild steel from corrosion to enhance its usage period. Various

studies have been conducted to study the anomalous codeposition behavior of NiCo alloy and found them good against corrosion protection of mild steel [34,35]. The anticorrosion behavior of NiZn and NiCo alloy was studied by Nady *et al.* [36] and reported the addition of organic substances like the gluconate salt and cysteine in the surface morphology and anticorrosion properties of the deposits.

Therefore, it would be interesting to combine the properties of Zn–Ni and Zn–Co alloys in one alloy which could be accomplished by the galvanostatic electrodeposition technique to see the effect of additive in corrosion inhibition of the deposited alloy coatings. The present work incorporated the synthesis of ternary Ni-Co-Zn alloy coating on mild steel substrate using galvanostatic electrochemical deposition technique from different deposition baths and the effect of pyridine as additive in deposition bath on corrosion resistance of deposited alloy coating. The properties of electrodeposited ternary Ni-Co-Zn alloy coatings were examined by different methods like SEM-EDAX and XRD and the Corrosion behavior of Ni-Co-Zn alloy coatings were observed by Tafel extrapolation method in two different acidic corrosive mediums i.e. 0.01 M HCl and 0.01 M H_2SO_4.

Materials and Methods

Cobalt sulphate heptahydrate ($CoSO_4.7H_2O$)Nickel Sulphate hexahydrate ($NiSO_4.6H_2O$), Zinc Sulphate monohydrate ($ZnSO_4.H_2O$), Sodium Sulphate (Na_2SO_4), boric acid (H_3BO_3), Trisodium citrate dehydrate ($Na_3C_6H_5O_7$), and pyridine (C_5H_5N) were supplied by Loba Chemia Pvt. Ltd. All chemical products were analytical and used directly.

Sample preparation

The Ni-Co-Zn alloy coatings were synthesized by galvanostatic electrochemical deposition in the different deposition baths of mixed solution containing metal sources and additives, as mentioned in Table 1, in conventional three electrode cell. In a three electrode electrochemical cell set up the mild steel sheets sealed with epoxy resin and by tapping with an exposure area 10 x 10 mm was used as working electrode. The saturated calomel electrode (SCE) was used as reference electrode and Mild Steel Plate is used as Counter electrode. Figure 1 (a) shows the diagrammatic representation of electrochemical deposition setup. Before electrochemical deposition, the mild steel sheets were polished with emery paper and cleaned in acetone and distilled water, respectively.

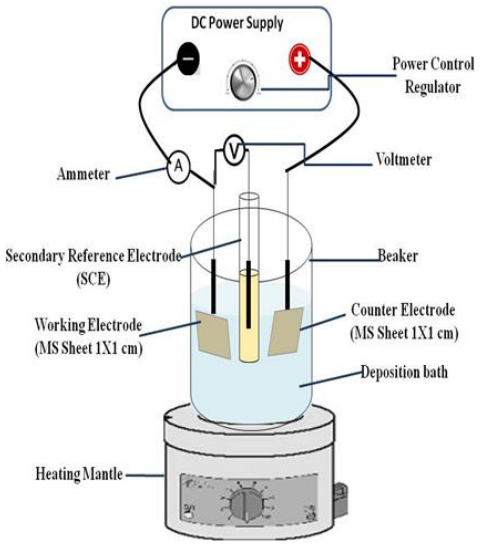

Figure 1 (a). Schematic diagram of ectrochemical setup for deposition of alloy coatings.

Figure 1 (b). Galvanostatic linear electrodeposition setup.

The deposition of alloy was carried out in conventional three-electrode cell which consists of calomel electrode as reference electrode. All potentials were referred to saturated calomel electrode. During the deposition process the high precision digital multimeters has been used for the measurement of current as well as potential and transistor based power supply was used for data acquisition. The diagrammatic representation of the deposition cell setup and the real image of electrodeposition set up are given in Figure 1(a) and 1(b). The film thickness was estimated using relationship:

$$F.T.= (I*t*eq.wt.) / (F*D*A) \quad (1)$$

Where,

F.T .= film thickness (cm)

Eq.wt.= equivalent weight of deposited alloy

I= current density (A/cm^2)

t = time (second)

F= faraday 's constant

D= density of alloy (gm/cm^3)

A= area of substrate (cm^2)

The minimum range of current density to be judged for the co-deposition of the metals has been decided by the current vs. potential graph, as shown in Figure 2.

After galvanostatic electrochemical deposition the Ni-Co-Zn alloy deposits were rinsed and air dried for investigation. For the testing of pyridine as corrosion inhibitor, C_5H_5N (40 ppm) was added into deposition bath containing mixed solution of metal sources and other additives under optimum deposition conditions. The different compositions of deposition baths and optimum deposition parameters are presented in Table 1. The galvanostatic electrochemical depositions were carried out for various deposition baths and after electrochemical deposition the Ni-Co-Zn deposits were rinsed and air dried for further investigation.

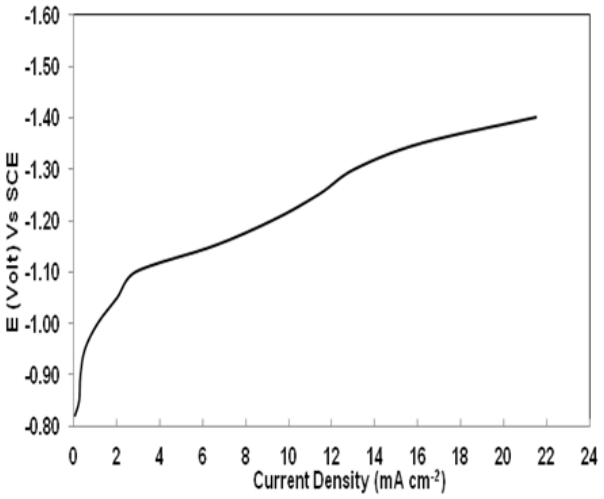

Figure 2. Current-potential curve for co-deposition of Ni-Co-Zn alloy coating.

Table 1. Deposition bath (DB) concentrations for the deposition of Ni-Co-Zn alloy coatings on MS substrate

Material	DB 1	DB 2	DB 3	DB 4
$NiSO_4.6H_2O$(mol/L)	0.1	0.1	0.1	0.1
$CoSO_4.7H_2O$(mol/L)	0.2	0.2	0.2	0.2
$ZnSO_4.H_2O$(mol/L)	0.2	0.3	0.2	0.3
Na_2SO_4 (mol/L)	0.2	0.2	0.2	0.2
H_3BO_3(mol/L)	0.2	0.2	0.2	0.2
$Na_3C_6H_5O_7$ (mol/L)	0.1	0.1	0.1	0.1
C_5H_5N (ppm)	-	-	40	40

Characterization

The surface morphologies of electrochemically deposited Ni-Co-Zn and Ni-Co-Zn_Py alloy coatings were examined by scanning electron microscopy using F Model: JEOL JSM5600 Scanning electron microscope with attached EDS model: INCA for detection of surface elemental composition. X-ray diffraction analysis of deposited alloy coatings was carried out by Bruker D8 Advance X-ray diffractometer. The X-rays of wavelength 1.54 Å (Cu K-alpha) were produced using a sealed tube and the X-rays were detected by Bruker LynxEye detector which is a fast counting detector based on Silicon strip technology. The crystallite size of the alloy particles is evaluated using the Scherrer's formula [37].

$$D = k\ \lambda / \beta\cos\theta \quad (1)$$

Where, k is known as Scherrer's constant which is 0.94, λ is the wavelength, and β is the full width at half maximum (FWHM) of high intensity diffraction peak in radians and θ is the angle of diffraction.

Broadening of the observed peak from the diffraction pattern was due to the defects. The strain induced broadening of peaks in XRD pattern is due to the imperfections and distortions which is described by Equation (2).

$$\varepsilon = \beta_o\ 4\tan\theta \quad (2)$$

Crystallite size and strain are two independent factors which hypothetically responsible for line broadening. the size and strain have Cauchy like profile, so the total peak broadening is basically the addition of Equations (1) and (2) and the resultant equation is known as Williamson-Hall (W–H) equation represented by both Equations (3) and (4) [38,39]:

$$\beta_0 = (k\ \lambda / \beta\cos\theta) + 4\ \varepsilon\tan\theta \quad (3)$$

or

$$\beta_0\ \cos\theta = (k\ \lambda / D) + 4\ \varepsilon\sin\theta \quad (4)$$

The anticorrosion competency of deposited Ni-Co-Zn coatings were characterized by electrochemical measurements performed in two different acid mediums i.e. 0.01 M HCl and 0.01 M H_2SO_4 using the three electrode cell manual set up as mentioned above at ambient temperature. The potentiodynamic polarization curve was recorded for both the anodic and cathodic polarization *vs* SCE.

The corrosion potential (E_{corr}) and corrosion current density (I_{corr}) were obtained using tafel extrapolation method and the corrosion rate is determined using the forumula given in Equation (5).

$$C.R. = (K.EW.i_{corr}) / (d.A) \quad (5)$$

Where,

C.R. = corrosion rate,

k= constant dependent on unit of Corrosion rate,

EW= equivalent weight of deposited alloy,

i_{corr} = Corrosion current density, d= density of deposited alloy and

A= area of substrate [40,41].

Results and Discussion

Ni-Co-Zn and Ni-Co-ZnPy alloy coatings prepared by electrochemical deposition

The suitable deposition current density was found to be 4 mA/cm² at which a visually even deposition layer was obtained for Ni-Co-Zn alloy (Figure 2). A variety of Zinc rich Ni-Co-Zn alloy coatings were prepared by electrodeposition at a current density of 4 mA/cm² in the different deposition baths for 20 minutes; which were apparent smooth, compact and thoroughly covered MS substrate. The coating obtained from deposition bath DB4 is the best adhere and even among all the coatings obtained from various deposition baths. No residues were spotted in any deposition bath after the deposition of alloy coatings. Addition of boric acid was beneficial to obtained zinc rich alloy thin films [42]. Boric acid formed complex with nickel and could absorbed on the surface of Zinc hydroxide and facilitate the development of Zinc rich alloy thin film [43,44]. The estimated film thickness is 0.235 micrometer.

The alloy coatings obtained from different deposition baths are abbreviated as follow:

Table 2. Alloy coatings deposited from various Deposition baths

Deposition Bath	Alloy coating
DB1	Ni-Co-$Zn_{0.20}$
DB2	Ni-Co-$Zn_{0.30}$
DB3	Ni-Co-$Zn_{0.20}$Py
DB4	Ni-Co-$Zn_{0.30}$Py

To know the surface morphology and the growth of alloy's crystalline particles the electrodeposited Ni-Co-Zn alloys at a constant current density of 4 mA/cm² from different baths have been studied and given in Figure 3.

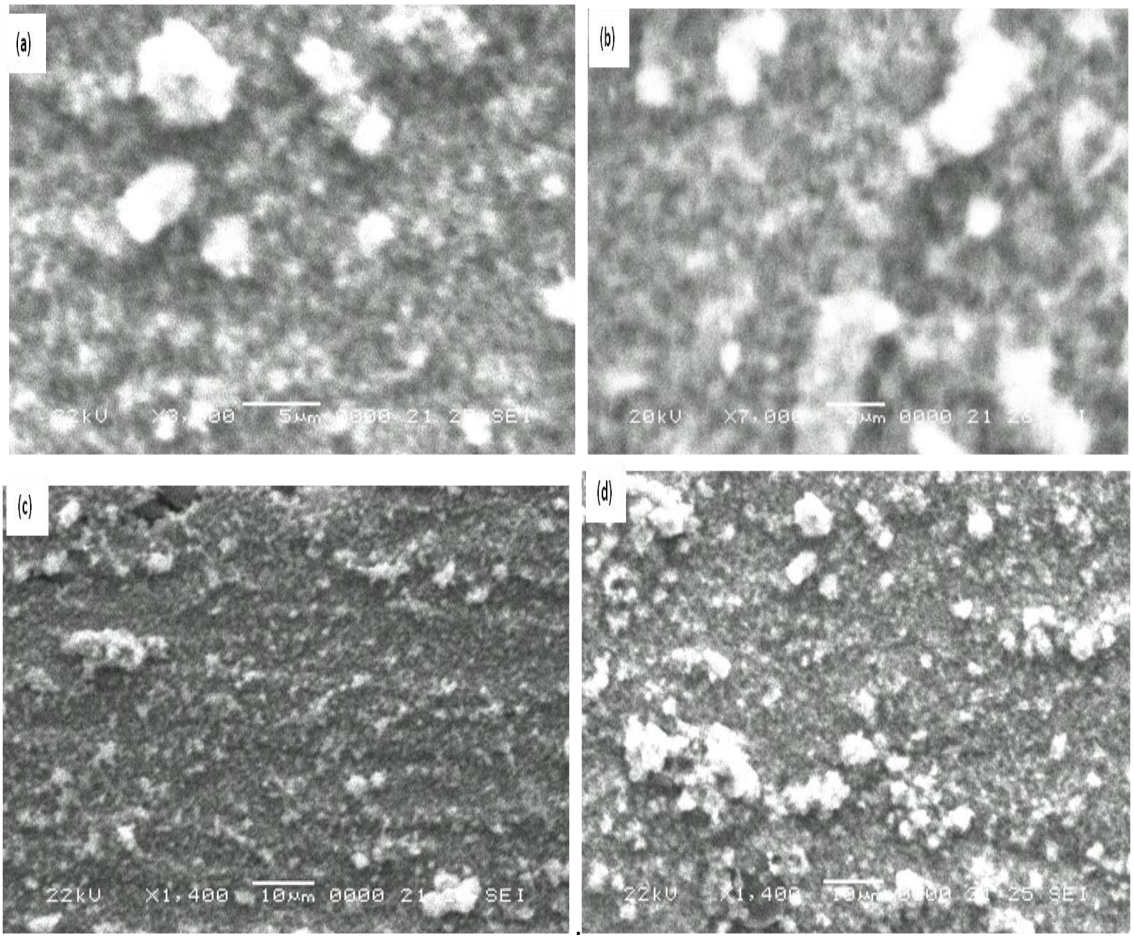

Figure 3. SEM images (a) Ni-Co-$Zn_{0.20}$ (b) Ni-Co-$Zn_{0.30}$, (c) Ni-Co-$Zn_{0.20}$Py, and (d) Ni-Co-$Zn_{0.30}$Py alloy coatings deposited on MS substrate.

It shows complete coverage of Mild Steel substrate by non-homogenously distributed NiCoZn alloy coating of asymmetrically ordered crystalline particles. Cauliflower shaped agglomerated particles are seen in all the samples of NiCoZn alloy coatings. There is no significant effect of increased concentration of zinc or addition of pyridine is seen on the shape of the crystalline particles only they appear denser and the particle size increased with increasing concentration of zinc and addition of pyridine. Figure 4 illustrates energy dispersive X-ray analysis of NiCoZn alloy coatings and confirms the percentage elemental composition of deposited alloy coatings. Less than 5% of Nickel and Cobalt is present while more than 50% Zinc is incorporated and remaining is oxygen content in the alloy coatings.

Table 3 contains the elemental composition of various deposited alloy coatings. Figure 5 shows the XRD pattern of Ni-Co-Zn coatings deposited at 4 mA/cm² on mild steel substrate. In XRD analysis, γ Zn-Ni phase is present predominantly in all the samples having maximum intensity of (330) plane around 44.60 (102) and (600) planes are also detected in Ni-Co-ZnO alloy samples.

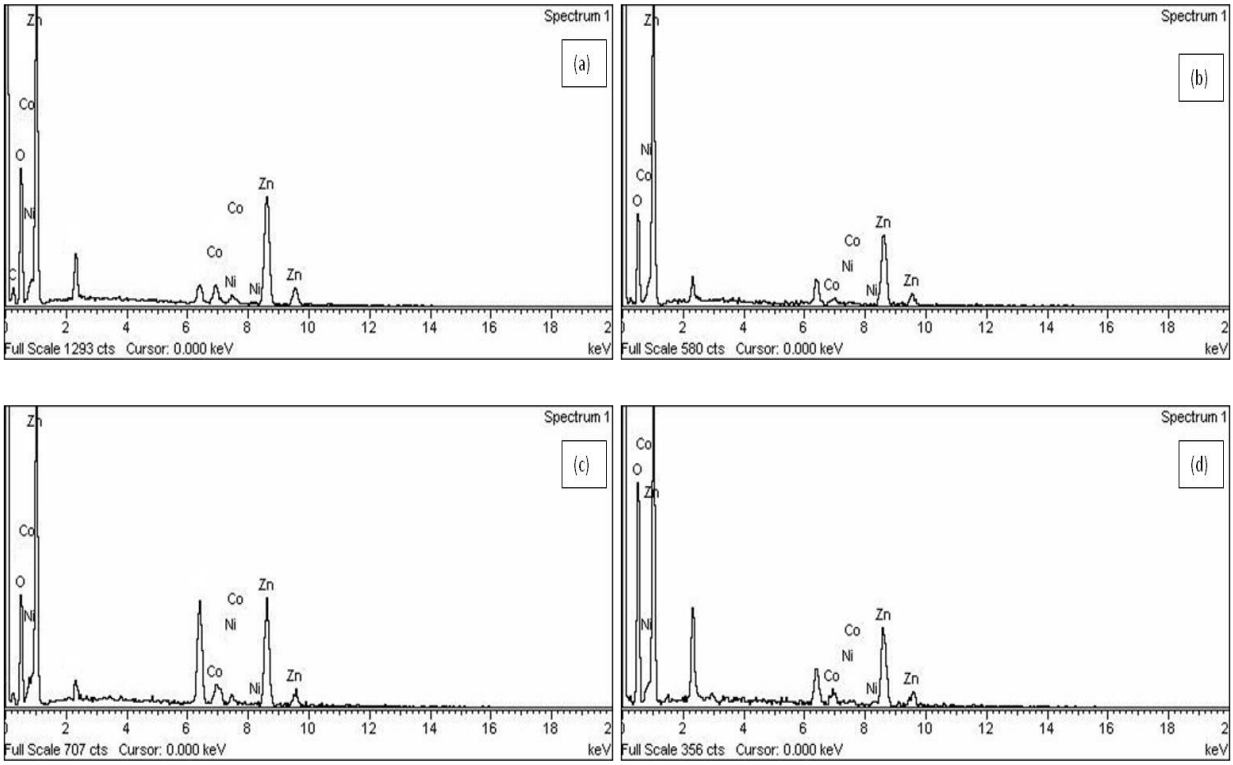

Figure 4. EDAX images (a) Ni-Co-$Zn_{0.20}$ (b) Ni-Co-$Zn_{0.30}$ (c) Ni-Co-$Zn_{0.20}$Py (d) Ni-Co-$Zn_{0.30}$Py alloy coatings deposited on MS substrate.

Table 3. Elemental composition of alloy coatings obtained by EDAX analysis

S. No.	Thin film sample	Percentage Nickel (Ni) content	Percentage Cobalt (Co) content	Percentage Zinc (Zn) content
1	Ni-Co-$Zn_{0.20}$	1.26	3.33	51.68
2	Ni-Co-$Zn_{0.30}$	0.41	0.48	64.94
3	Ni-Co-$Zn_{0.20}$Py	3.09	2.67	45.61
4	Ni-Co-$Zn_{0.30}$Py	0.45	3.17	48.55

Peaks of η Zn were further seen in the tested samples which are confirmed by comparing it with International Centre for Diffraction Database (JCPDS file# 00-004-0031 and PDF# 03-065 respectively). For Ni-Co-$Zn_{0.30}$ alloy coating the most intense peak is obtained for η Zn phase for (100) plane at 38.35°, this is due to greater increment of concentration of Zinc in the coating as compared to the Ni content [45]. Additional ZnO crystalline phase (PDF# 80-0075) for (100) and (103) plane is present around 31.84° and 61.23° due to the higher percentage content of zinc in the Ni-Co-$Zn_{0.30}$ alloy coating [46]. The peaks corresponding to pure cobalt or Nickel were not viewed in the XRD patterns; it is a sign of the co-existence of the metals on different planes of crystalline phase which indicate the formation of homogeneous solid solution of stable structured NiCoZn alloy [47]. Figure 6 (a)-(d) have Williamson-Hall analysis of Ni-Co-Zn alloy coatings to justify the peak broadening and to find out the strain of the film coatings. The peak broadening indicated the reduction of crystallite size of the Zn-Ni-Co alloy coatings [46]. The highest 97.64 nm crystallite size was calculated for Ni-Co-$Zn_{0.30}$Py by Williamson-Hall analysis. Higher zinc concentration is responsible for greater strain of the Ni-Co-Zn alloy thin film and the addition of organic inhibitor also generate higher strained alloy coatings than the Ni-Co-Zn synthesized in absence of organic inhibitor Pyridine. Table 4 contains the Scherrer's method and Williamson-Hall plot data of Ni-Co-Zn alloy coatings.

Corrosion analysis of deposited Ni-Co-Zn alloy coatings

To estimate the corrosion protection of electrodeposited Ni-Co-Zn coating in presence of pyridine the potentiodynamic polarization curves were obtained in 0.01 M HCl solution medium and 0.01 M H_2SO_4 solution, applied as corrosive medium and obtained results were

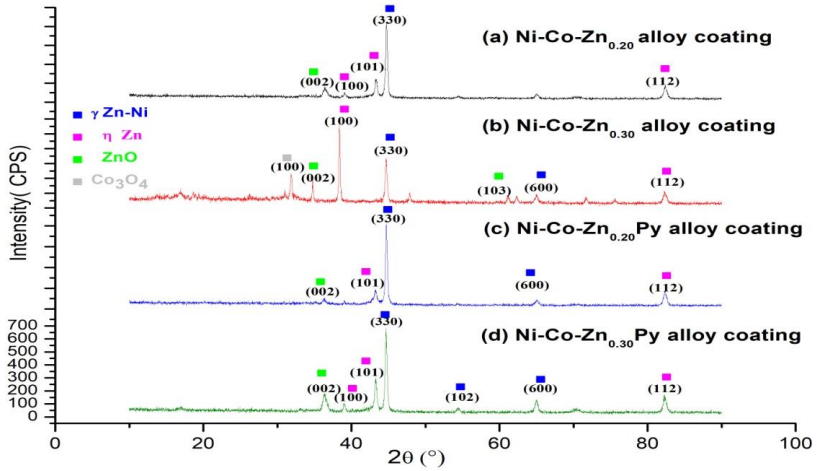

Figure 5. XRD of Ni-Co-Zn alloy coatings.

Table 4. Scherrer's method and Williamson-Hall analysis data of Ni-Co-Zn alloy coatings

Ni Co Zn Alloy coatings	Scherrer's Method		Williamson Hall Analysis	
	Crystallite Size D (nm)	δ x 10^{-3}	D (nm)	ε_α x 10^{-3}
Ni-Co-$Zn_{0.20}$	29.08	1.18	35.55	1.33
Ni-Co-$Zn_{0.30}$	44.20	0.51	88.88	1.66
Ni-Co-$Zn_{0.20}$Py	30.09	1.10	97.64	2.56
Ni-Co-$Zn_{0.30}$Py	25.35	1.56	27.29	5.36

shown in Figure 7 (a) and (b). The electrochemical parameters i.e. corrosion potential (E_{corr}) and Corrosion Current density (I_{corr}) were derived from potentiodynamic polarization curves using Tafel extrapolation method and corrosion rate (C.R.) as well as percentage inhibiter efficiency (I.E.) were calculated using the derived data from potentiodynamic polarization curves and summarized in Tables 5 and 6.

The % inhibitor efficacy has been calculated using the following equation:

Inhibitor efficacy (%)= 100 . {(C.R. $_{uninhibited}$ - C.R. $_{inhibited}$)/ C.R. $_{uninhibited}$} (6)

It is observed that the corrosion rate obtained in Ni-Co-$Zn_{0.30}$ and Ni-Co-$Zn_{0.30}$Py alloy coatings obtained from deposition baths DB2 and DB4 is lower than the coatings obtained from DB1 and DB3. The inhibition efficacy of pyridine is better in HCl medium as compared to H_2SO_4 medium.

Pyridine is a good corrosion inhibitor for Ni-Co-Zn alloy thin films in HCl medium. The minimum of 0.0827 $mmyr^{-1}$ corrosion rate in HCl medium is obtained for $NiCoZn_{0.30}$ alloy synthesized in presence of pyridine. 66.48% I.E. is shown by $NiCoZn_{0.30}$ alloy coating in HCl medium, as observed in Figure 7 which shows the comparison of I.E. of pyridine in different mediums for different alloy coatings. Pyridine worked as moderate corrosion inhibitor for Ni-Co-Zn alloy coating in H_2SO_4 medium. In H_2SO_4 corrosive medium, the maximum of 40.42% inhibitor efficiency has been found for $NiCoZn_{0.30}$ alloy coating. It has been observed that the corrosion rate decreases with increase in Zinc percentage in deposited alloy.

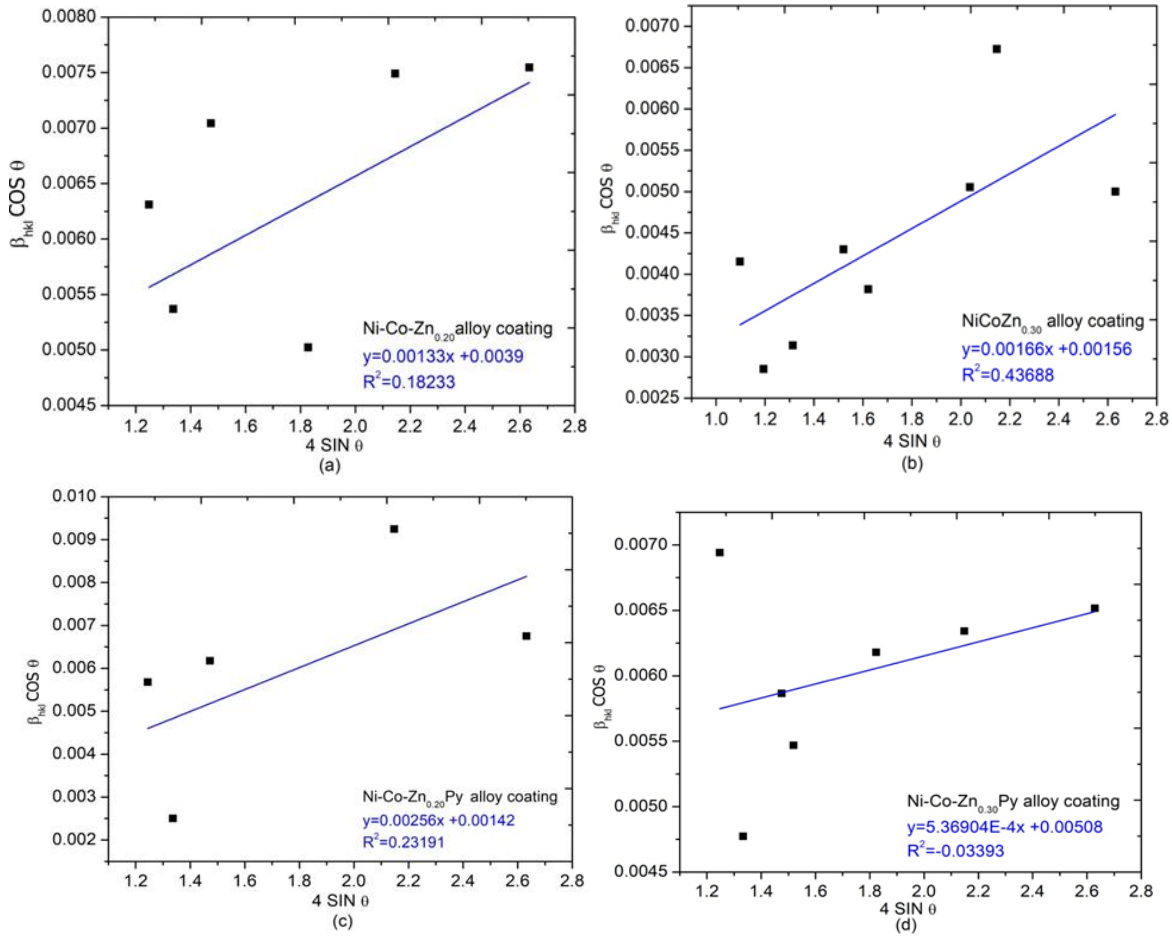

Figure 6. Williamson-Hall plots for NiCoZn alloy thin films (a-d).

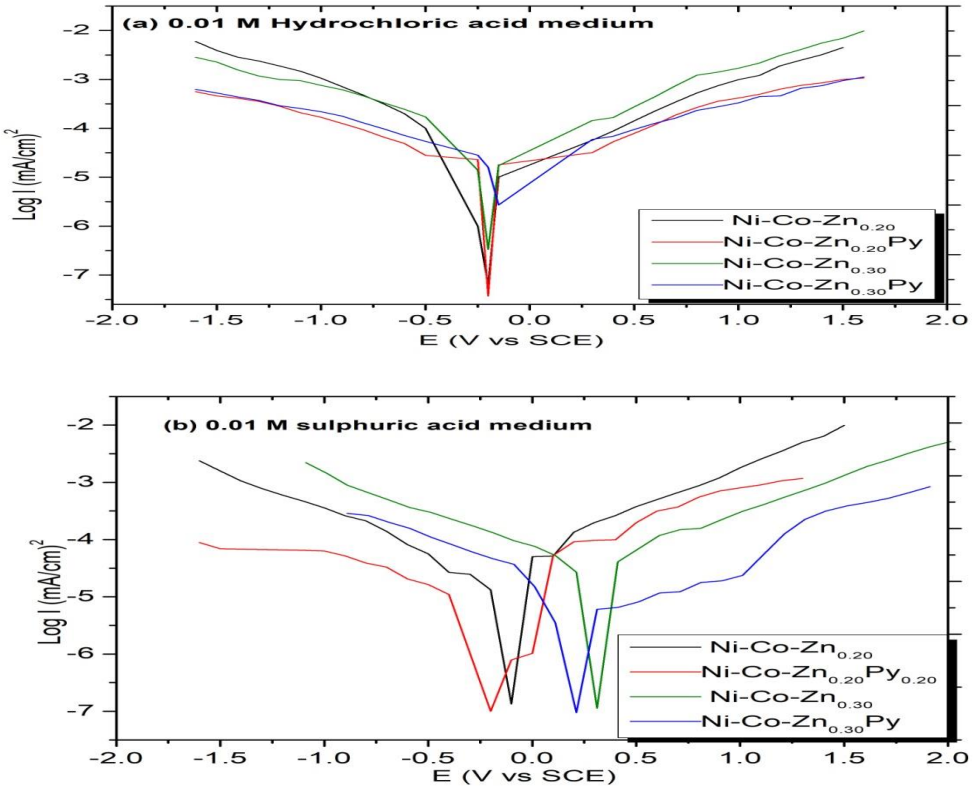

Figure 7. Tafel polarization curves for Ni-Co-Zn alloy coatings (a) in 0.01 M hydrochloric acid corrosive medium (b) in 0.01 M sulphuric acid corrosive medium.

Table 5. Corrosion data of Ni-Co-Zn coatings in 0.01 M HCl corrosive medium

Ni-Co-Zn alloy coating	Alloy coating synthesize in absence of pyridine			Ni-Co-Zn alloy coating	Alloy coating synthesize in presence of pyridine			Inhibitor efficiency (%)
	E_{corr} (V)	I_{corr} (A/cm^2)	Corrosion rate (mm/yr)		E_{corr} (V)	I_{corr} (A/cm^2)	Corrosion rate (mm/yr)	
Ni-Co-Zn$_{0.20}$	-0.208	1.59X 10^{-05}	0.2327	Ni-Co-Zn$_{0.20}$Py	-0.200	1.00X 10^{-05}	0.1557	36.91
Ni-Co-Zn$_{0.30}$	-0.200	1.58X 10^{-05}	0.2326	Ni-C o-Zn$_{0.30}$Py	-0.136	5.31X 10^{-06}	0.0827	66.48

Table 6. Corrosion data of Ni-Co-Zn alloy coatings in 0.01 M H_2SO_4 corrosive medium

Ni-Co-Zn alloy coating	Alloy coating synthesize in absence of Pyridine			Ni-Co-Zn alloy coating	Alloy coating synthesize in presence of pyridine			Inhibitor efficiency (%)
	E_{corr} (V)	I_{corr} (A/cm^2)	Corrosion rate (mm/yr)		E_{corr} (V)	I_{corr} (A/cm^2)	Corrosion rate (mm/yr)	
Ni-Co-Zn$_{0.20}$	-0.105	4.22 X 10^{-05}	0.6196	Ni-Co-Zn$_{0.20}$Py	-0.200	2.66 X 10^{-05}	0.4144	36.94
Ni-Co-Zn0.30	- 0.073	2.11 X 10^{-05}	0.3103	Ni-Co-Zn$_{0.30}$Py	-0.160	1.26X 10^{-05}	0.1960	40.42

Pyridine is a good corrosion inhibitor for Ni-Co-Zn alloy thin films in HCl medium. The minimum of 0.0827 mmyr^{-1} corrosion rate in HCl medium is obtained for $NiCoZn_{0.30}$ alloy synthesized in presence of pyridine. 66.48% I.E. is shown by $NiCoZn_{0.30}$ alloy coating in HCl medium, as observed in Figure 7 which shows the comparison of I.E. of pyridine in different mediums for different alloy coatings. Pyridine worked as moderate corrosion inhibitor for Ni-Co-Zn alloy coating in H_2SO_4 medium. In H_2SO_4 corrosive medium, the maximum of 40.42% inhibitor efficiency has been found for $NiCoZn_{0.30}$ alloy coating. It has been observed that the corrosion rate decreases with increase in Zinc percentage in deposited alloy. Figure 8 shows the comparison of inhibitor efficiency (%IE) mentioned in Tables 3 and 4. The % IE of pyridine is better in zinc rich Ni-Co-$Zn_{0.30}$Py alloy coating in both corrosive mediums, as compared to Ni-Co-$Zn_{0.30}$ alloy coating which clearly states the greater anticorrosive behavior of the Ni-Co-$Zn_{0.30}$Py alloy coating as compared to other deposited coatings.

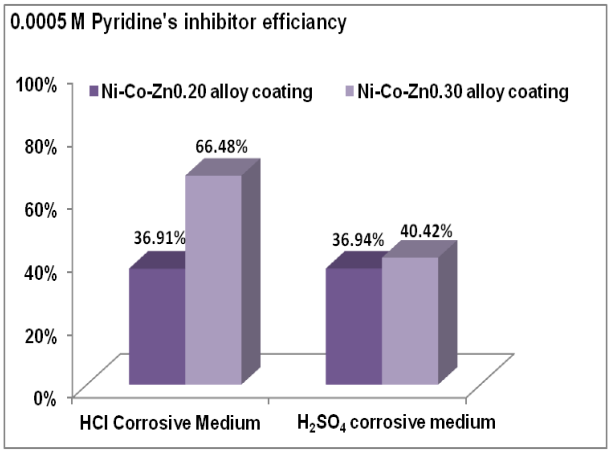

Figure 8. Inhibitor efficiency of Pyridine for NiCoZn alloy coatings in different mediums.

Conclusion

Galvanostatic electrodeposition and corrosion studies of different NiCoZn alloy thin coatings on mild steel substrate are presented. The NiCoZn thin coatings with different percentage composition were deposited using different sulphate-citrate baths in presence and absence of Pyridine on 4 mA/cm^2 for 20 minutes. The addition of pyridi ne strengthened the anticorrosion property of NiCoZn alloy thin coatings. All the deposited coatings are visually intact and evenly coated the mild steel substrate. Scanning electron microscopy confirmed the nonhomogenously coated MS substrate with NiCoZn coatings having agglomerated cauliflower like particles and EDAX analysis illustrated the zinc rich NiCoZn coatings on MS Substrate. Structural analysis of NiCoZn alloy coatings on MS substrate by XRD method corroborated the inter diffusion of Nickel , Cobalt and zinc phases and confirmed the presence of some phases i.e. Epsilon Co, FCC Ni(Co), η Zn, γ Zn-Ni, and Co_3O_4. The average crystallite size for all deposited thin coatings did not excided than 100 nm and the strain obtained by size-strain plot method in all the thin coatings is less than 5. The higher amount of Zinc and incorporation of pyridine leaded the more strained alloy thin coatings. The electrochemical tafel polarization measurements demonstrated the excellent corrosion resistance of Pyridine reinforced NiCoZn alloy thin coatings as compared to simple NiCoZn alloy thin coatings on Mild steel substrate in 0.01 M acidic mediums. Incorporation of heteroatom of pyridine with NiCoZn thin coating may endow barrier between corrosive medium and coating to provide better corrosion protection to substrate containing thin coating. To know the mechanism of corrosion protection by additive pyridine further investigation should be conducted.

Acknowledgements

The authors would like to thank director of UGC-DAE CSR, Indore for given the permission to conduct characterization techniques in UGC-DAE Consortium. They would also like to

acknowledge Dr. D. M. Phase and Dr. Mukul Gupta for providing facility to conduct surface characterization and XRD analysis of alloy thin film coatings in UGC-DAE CSR, Indore.

Conflict of Interest

The authors declare that they have no competing financial interests or personal relationships that could have appeared to influence the work reported in this paper.

Orcid

Shraddha Bais : 0000-0001-7040-5933

References

[1] A. Karimzadeh, M. Aliofkhazraei, F.C. Walsh, A review of electrodeposited Ni-Co alloy and composite coatings: Microstructure, properties and applications, *Surface and Coatings Technology*, **2019**, *372*, 463-498. [Crossref], [Google Scholar], [Publisher]

[2] M. Hu, Q. Cao, X. Wang, D. Zhang, J.-Z. Jiang, Ultra-strong nanostructured Co-Ni-V medium entropy alloy thin film designed by interface strengthening, *Thin Solid Films*, **2021**, *734*, 138866. [Crossref], [Google Scholar], [Publisher]

[3] M. Kamel, E. Alzahrani, I. Ibrahim, S. Rashwan, Electrodeposition of well-crystalline Ni-Co alloy thin films on steel substrates from aqueous solutions containing citrate anions, *International Journal of Electrochemical Science*, **2021**, *16*, 210942. [Crossref], [Google Scholar], [Publisher]

[4] I. Dul, Application and processing of nickel alloys in the aviation industry, *Welding International*, **2013**, *27*, 48-56. [Crossref], [Google Scholar], [Publisher]

[5] S. Khorsand, K. Raeissi, F. Ashrafizadeh, M. Arenas, A. Conde, Corrosion behaviour of super-hydrophobic electrodeposited nickel–cobalt alloy film, *Applied Surface Science*, **2016**, *364*, 349-357. [Crossref], [Google Scholar], [Publisher]

[6] M.N. Raveendran, A.C. Hegde, Anomalous codeposition of NiCo alloy coatings and their corrosion behaviour, *Materials Today: Proceedings*, **2022**, *62*, 5047-5052. [Crossref], [Google Scholar], [Publisher]

[7] O. Hammami, L. Dhouibi, E. Triki, Influence of Zn–Ni alloy electrodeposition techniques on the coating corrosion behaviour in chloride solution, *Surface and Coatings Technology*, **2009**, *203*, 2863-2870. [Crossref], [Google Scholar], [Publisher]

[8] K. Sriraman, S. Brahimi, J. Szpunar, J. Osborne, S. Yue, Characterization of corrosion resistance of electrodeposited Zn–Ni Zn and Cd coatings, *Electrochimica Acta*, **2013**, *105*, 314-323. [Crossref], [Google Scholar], [Publisher]

[9] H. Joress, B. DeCost, N. Hassan, T.M. Braun, J.M. Gorham, J. Hattrick-Simpers, Development of an automated millifluidic platform and data-analysis pipeline for rapid electrochemical corrosion measurements: A pH study on Zn-Ni, *Electrochimica Acta*, **2022**, *428*, 140866. [Crossref], [Google Scholar], [Publisher]

[10] R. Zellagui, H. Dehdouh, M. Adnane, M.S. Akhtar, M. Saeed, CdxZn1-xS thin films deposited by chemical bath deposition (CBD) method, *Optik*, **2020**, *207*, 164377. [Crossref], [Google Scholar], [Publisher]

[11] S. Battiato, A.L. Pellegrino, A. Pollicino, A. Terrasi, S. Mirabella, Composition-controlled chemical bath deposition of Fe-doped NiO microflowers for boosting oxygen evolution reaction, *International Journal of Hydrogen Energy*, **2023**, *48*, 18291-18300. [Crossref], [Google Scholar], [Publisher]

[12] F. Bignoli, S. Rashid, E. Rossi, S. Jaddi, P. Djemia, G. Terraneo, A.L. Bassi, H. Idrissi, T. Pardoen, M. Sebastiani, Effect of annealing on mechanical properties and thermal stability of ZrCu/O nanocomposite amorphous films

synthetized by pulsed laser deposition, *Materials & Design*, **2022**, *221*, 110972. [Crossref], [Google Scholar], [Publisher]

[13] A. Dawood, N. Ahmed, S. Bashir, A. Hayat, S.M.A. Sarfraz, A. Ayub, Laser ablation of copper alloy under varying environmental conditions to achieve purpose-built surface structures, *Coatings*, **2022**, *12*, 1972. [Crossref], [Google Scholar], [Publisher]

[14] Z. Zhou, B. Liu, W. Guo, A. Fu, H. Duan, W. Li, Corrosion behavior and mechanism of FeCrNi medium entropy alloy prepared by powder metallurgy, *Journal of Alloys and Compounds*, **2021**, *867*, 159094. [Crossref], [Google Scholar], [Publisher]

[15] W. Xu, X. Lu, J. Tian, C. Huang, M. Chen, Y. Yan, L. Wang, X. Qu, C. Wen, Microstructure, wear resistance, and corrosion performance of $Ti_{35}Zr_{28}Nb$ alloy fabricated by powder metallurgy for orthopedic applications, *Journal of Materials Science & Technology*, **2020**, *41*, 191-198. [Crossref], [Google Scholar], [Publisher]

[16] J. Jiang, Y. Sun, Y. Chen, Q. Zhou, H. Rong, X. Hu, H. Chen, L. Zhu, S. Han, Ultrasonic-assisted Ni–Mo–P doping hydrothermal synthesis of clustered spherical MoS_2 composite coating: wear and corrosion resistance, *Surface Engineering*, **2020**, *36*, 889-899. [Crossref], [Google Scholar], [Publisher]

[17] H. Firouzi-Nerbin, F. Nasirpouri, E. Moslehifard, Pulse electrodeposition and corrosion properties of nanocrystalline nickel-chromium alloy coatings on copper substrate, *Journal of Alloys and Compounds*, **2020**, *822*, 153712. [Crossref], [Google Scholar], [Publisher]

[18] JJ.A.M. Oliveira, A.F. de Almeida, A.R.N. Campos, S. Prasad, J.J.N. Alves, R.A.C. de Santana, Effect of current density, temperature and bath pH on properties of Ni–W–Co alloys obtained by electrodeposition, *Journal of Alloys and Compounds*, **2021**, *853*, 157104. [Crossref], [Google Scholar], [Publisher]

[19] Y. Li, X. Cai, G. Zhang, C. Xu, W. Guo, M. An, Optimization of electrodeposition nanocrytalline Ni-Fe alloy coatings for the replacement of Ni coatings, *Journal of Alloys and Compounds*, **2022**, *903*, 163761. [Crossref], [Google Scholar], [Publisher]

[20] K.K. Maniam, S. Paul, Corrosion performance of electrodeposited zinc and zinc-alloy coatings in marine environment, *Corrosion and Materials Degradation*, **2021**, *2*, 163-189. [Crossref], [Google Scholar], [Publisher]

[21] F. Zucchi, Book Review: Organic Inhibitors of Corrosion Metals. Yurii I. Kuznetsov. Plenum Publishing Corporation, New York, *Corrosion*, **1997**, *39*, 1145-1146. [Crossref], [Google Scholar], [Publisher]

[22] H. Tian, Y.F. Cheng, Novel inhibitors containing multi-functional groups for pipeline corrosion inhibition in oilfield formation water, *Corrosion*, **2016**, *72*, 472-485. [Crossref], [Google Scholar], [Publisher]

[23] P.I. Murungi, A.A. Sulaimon, Ideal corrosion inhibitors: a review of plant extracts as corrosion inhibitors for metal surfaces, *Corrosion Reviews*, **2022**, *40*, 127-136. [Crossref], [Google Scholar], [Publisher]

[24] A. Kokalj, Corrosion inhibitors: Physisorbed or chemisorbed?, *Corrosion Science*, **2022**, *196*, 109939. [Crossref], [Google Scholar], [Publisher]

[25] H.M.A. El-Lateef, A.-R. El-Sayed, H.S. Mohran, H.A.S. Shilkamy, Corrosion inhibition and adsorption behavior of phytic acid on Pb and Pb–In alloy surfaces in acidic chloride solution, *International Journal of Industrial Chemistry*, **2019**, *10*, 31-47. [Crossref], [Google Scholar], [Publisher]

[26] Z. Li, Q. Ren, X. Wang, Q. Kuang, D. Ji, R. Yuan, X. Jing, Effect of phosphate additive on the morphology and anti-corrosion performance of plasma electrolytic oxidation coatings on magnesium—lithium alloy, *Corrosion Science*,

2019, *157*, 295-304. [Crossref], [Google Scholar], [Publisher]

[27] U.P. Kumar, S. Shanmugan, C.J. Kennady, S. Shibli, Anti-corrosion and microstructural properties of Ni–W alloy coatings: Effect of 3, 4-dihydroxybenzaldehyde, *Heliyon*, **2019**, *5*. [Crossref], [Google Scholar], [Publisher]

[28] K. Auepattana-Aumrung, T. Phakkeeree, D. Crespy, Polymer-corrosion inhibitor conjugates as additives for anticorrosion application, *Progress in Organic Coatings*, **2022**, *163*, 106639. [Crossref], [Google Scholar], [Publisher]

[29] W. Zhang, D. Zhang, X. Li, C. Li, L. Gao, Excellent performance of dodecyl dimethyl betaine and calcium gluconate as hybrid corrosion inhibitors for Al alloy in alkaline solution, *Corrosion Science*, **2022**, *207*, 110556. [Crossref], [Google Scholar], [Publisher]

[30] M. Mobin, M. Parveen, R. Aslam, Effect of different additives, temperature, and immersion time on the inhibition behavior of L-valine for mild steel corrosion in 5% HCl solution, *Journal of Physics and Chemistry of Solids*, **2022**, *161*, 110422. [Crossref], [Google Scholar], [Publisher]

[31] H.M. Abd El-Lateef, A.R. Sayed, K. Shalabi, Studying the effect of two isomer forms thiazole and thiadiazine on the inhibition of acidic chloride-induced steel corrosion: Empirical and Computer simulation explorations, *Journal of Molecular Liquids*, **2022**, *356*, 119044. [Crossref], [Google Scholar], [Publisher]

[32] R. Aslam, G. Serdaroglu, S. Zehra, D.K. Verma, J. Aslam, L. Guo, C. Verma, E.E. Ebenso, M. Quraishi, Corrosion inhibition of steel using different families of organic compounds: Past and present progress, *Journal of Molecular Liquids*, **2022**, *348*, 118373. [Crossref], [Google Scholar], [Publisher]

[33] E. McCafferty, Introduction to corrosion science, Springer Science & Business Media, **2010**. [Google Scholar], [Publisher]

[34] Y. Jiang, C.Y. Chen, T. Kurioka, X. Luo, D. Yamane, M. Sone, T.M. Chang, Effects of bromide ions in anomalous codeposition of Ni-Co alloys with a sulfamate based electrolyte, *Journal of The Electrochemical Society*, **2023**, *170*, 072507. [Crossref], [Google Scholar], [Publisher]

[35] Y. Xue, S. Wang, G. Zhao, A. Taleb, Y. Jin, Fabrication of NiCo coating by electrochemical deposition with high super-hydrophobic properties for corrosion protection, *Surface and Coatings Technology*, **2019**, *363*, 352-361. [Crossref], [Google Scholar], [Publisher]

[36] H. Nady, M. Negem, Microstructure and corrosion behavior of electrodeposited NiCo, NiZn and NiCu nanocrystalline coatings in alkaline solution, *Zeitschrift für Physikalische Chemie*, **2017**, *231*, 1159-1178. [Crossref], [Google Scholar], [Publisher]

[37] B.D. Cullity, Elements of X-ray differection, Addision- Wesley Publishing Company, 2007.

[38] G. Williamson, W. Hall, X-ray line broadening from filed aluminium and wolfram, *Acta Metallurgica*, **1953**, *1*, 22-31. [Crossref], [Google Scholar], [Publisher]

[39] L.V. Azaroff, Element of X-ray crystallography, McGraw-Hill: New York, **1968**. [Google Scholar]

[40] R.A. Buchanan, E.E. stansbury, A.S.M. Internationals, **2000**, p. 233. [Google Scholar]

[41] B.N. Popov, Corrosion Engineering-principles and solved problems, Elsevier, **2015**, p. 233. [Google Scholar]

[42] A. Brenner, Electrodeposition of alloys, **1963**. [Crossref], [Google Scholar], [Publisher]

[43] S. Vivegnis, M. Krid, J. Delhalle, Z. Mekhalif, F. Renner, Use of pyrophosphate and boric acid additives in the copper-zinc alloy electrodeposition and chemical dealloying, *Journal of Electroanalytical Chemistry*, **2019**,

848, 113310. [Crossref], [Google Scholar], [Publisher]

[44] Y.E. Sknar, I. Sknar, O. Savchuk, F. Danilov, Electrodeposition of NiCo alloy from methansulfonate electrolyte. The role of the electrolyte pH in the anomalous codeposition of nickel and cobalt, *Surface and Coatings Technology*, **2020**, *387*, 125542. [Crossref], [Google Scholar], [Publisher]

[45] J.S. Kavirajwar, S. Basavanna, B.K. Devendra, An investigation on corrosion properties of bright Zn-Ni alloy coated mild steel, *Electrochemical Science Advances*, **2022**, *2*, e2100097. [Crossref], [Google Scholar], [Publisher]

[46] P.S. Sundaram, T. Sangeetha, S. Rajakarthihan, R. Vijayalaksmi, A. Elangovan, G. Arivazhagan, XRD structural studies on cobalt doped zinc oxide nanoparticles synthesized by coprecipitation method: Williamson-Hall and size-strain plot approaches, *Physica B: Condensed Matter*, **2020**, *595*, 412342. [Crossref], [Google Scholar], [Publisher]

[47] N. Wang, T. Hang, S. Shanmugam, M. Li, Preparation and characterization of nickel–cobalt alloy nanostructures array fabricated by electrodeposition, *CrystEngComm*, **2014**, *16*, 6937-6943. [Crossref], [Google Scholar], [Publisher]

HOW TO CITE THIS ARTICLE

S. Bais. Fabrication of Electrochemically Deposited Zinc Rich Ni-Co-Zn Alloy Coatings Reinforced with Pyridine and Investigation of Their Anticorrosion Performance in Acidic Mediums. *Adv. J. Chem. A*, 2024, 7(5), 550-564.

DOI: 10.48309/AJCA.2024.450766.1508
URL: https://www.ajchem-a.com/article_196937.html